Biophysical Journal
Article

Biophysical Society

Restitution and Stability of Human Ventricular Action Potential at High and Variable Pacing Rate

Massimiliano Zaniboni[1,*]
[1]University of Parma, Department of Chemistry, Life Sciences and Environmental Sustainability, Parma, Italy

ABSTRACT Despite the key role of beat-to-beat action potential (AP) variability in the onset of ventricular arrhythmias at high pacing rate, the knowledge of the involved dynamics and of effective prognostic parameters is largely incomplete. Electrical restitution (ER), the way AP duration (APD) senses changes in preceding cycle length (CL), has been used to monitor transition to arrhythmias. The use of standard ER (sER), though, is controversial, not always suitable for in vivo and only rarely for clinical applications. By means of simulations on a human ventricular AP model, I investigate the dynamics of APD at high pacing rate under sinusoidally, saw-tooth, and randomly variable pacing CLs. AP sequences were compared in terms of beat-to-beat restitution (btb-ER) and of the collections of sER curves generated from each beat. A definition of APD stability is also proposed, based on successive APD changes introduced in an AP sequence by a premature beat. The explored CL range includes values leading to APD alternans under constant pacing. Three different types of response to CL variability were found, corresponding to progressively higher rate of beat-to-beat CL changes. Low rates (~1 ms/beat) generate a btb-ER dominated by steady-state rate dependence of APD (type 1), intermediate rates (~5 ms/beat) lead to a btb-ER similar to a single sER (type 2), and high rates (~20 ms/beat) to hysteretic btb-ER under periodic pacing and to a vertically spread btb-ER in the case of random pacing (type 3). Stability of AP repolarization always increases with the rate of CL changes. Thus, rather than looking at sER slope, which requires additional interventions during the recording of cardiac electrical activity, this study provides rationale for the use of btb-ER representations as predictors of repolarization stability under extreme pacing conditions, known to be critical for the arrhythmia development.

SIGNIFICANCE In this study, I propose to use a combination of electrical restitution measurements to characterize stability of action potential repolarization under high and beat-to-beat variable pacing rate, conditions known to be critical for transition from normal sinus rhythm to tachyarrhythmias. I discuss three different responses of human cardiac ventricular repolarization under sinusoidally, saw-tooth, and randomly varying pacing cycle length, based on beat-to-beat relationship between action potential duration and cycle length. This type of approach, compared to others more technically demanding, represents a suitable tool to monitor and understand repolarization stability under fast pacing conditions and can provide a significant dynamic marker for better fitting existing cardiac action potential models to experimental data and a target for developing new antiarrhythmic strategies.

INTRODUCTION

The repolarization of cardiac ventricular action potential (AP) is intrinsically a beat-to-beat variable, even at the cellular level and at constant pacing rate (1). Variability takes the form of alternans of AP duration (APD) at high constant pacing rate, at which it is frequently associated with an increased susceptibility to tachyarrhythmias or fibrillation (2). Constant pacing rate, though, is not a physiological condition because heart rate varies on a beat-to-beat basis, and indeed, the absence of variability indicates a poor prognosis (3). Heart rate variability affects APD variability (4), and its disturbances, e.g., in the form of pre- or postmature beats, are potentially arrhythmogenic (5).

The way APD adapts to preceding CL changes is called electrical restitution (ER). This is measured in its standard form (sER) with the so-called S1S2 protocol by estimating APD alterations after a sudden change in pacing cycle length (CL) after conditioning at constant pacing rate (6). It can also be measured as beat-to-beat restitution (btb-ER) by reporting, for an AP sequence at variable pacing rate, each APD as a function of the preceding CL (btb-ER_{CL})

Submitted April 16, 2019, and accepted for publication August 19, 2019.
*Correspondence: massimiliano.zaniboni@unipr.it
Editor: Kenneth Campbell.
https://doi.org/10.1016/j.bpj.2019.08.020

or of the preceding diastolic interval (DI) (btb-ER_{DI}) (4,7,8). The interest of basic cardiac electrophysiology and of clinical practice in ER is based on the restitution hypothesis, which identifies in the slope of the sER curve a threshold parameter for the stable or unstable development of sudden changes in CL (9). There are, though, several points concerning ER measurements that still need to be clarified. Firstly, the restitution hypothesis is strictly defined at constant pacing conditions (10), which is hardly the case of in vivo measurements. Also, although in clinical practice sER is more frequently measured (11,12), it is btb-ER that better captures APD dynamics during transition from tachyarrhythmias to VF (13,14). The difference between the two types of measures has been discussed recently (14,15) by pointing to the different mechanisms underlying the two phenomena.

Koller and co-workers first proposed as responsible for the difference between sER and btb-ER the cardiac memory, a slowly (seconds to minutes) accumulating influence of past pacing history on AP dynamics (13). I have recently discussed the mechanism of short-term (few beats) AP memory, which determines the morphology of btb-ER and becomes significant at high pacing rate and for large beat-to-beat CL changes, in which it is involved in the stability of AP repolarization (16). It is at these extreme pacing conditions that btb-ER assumes a hysteretic form, when the states of consecutive beats (CL_{n-1}, APD_n) move on a family of instead of on only one sER curve, thus leading to hysteresis in btb-ER representation.

The way pacing variability affects APD variability by modulating the stability of AP repolarization has been studied extensively. In a model study on the ten Tusscher et al. ventricular AP model (17), Dvir and Zlochiver have found that pacing stochasticity moderately reduces the slope of sER_{DI} but significantly suppresses the occurrence of concordant APD alternans, rendering the tissue less arrhythmogenic (18). They subsequently showed that intracellular sodium transient, already known to be involved in short-term cardiac AP memory (19), plays a key role in the antiarrhythmic effect of stochastic pacing (20). The most life-threatening of the cardiac arrhythmias is ventricular fibrillation (VF). A recognized key factor in precipitating the transition to VF is the appearance in the electrocardiogram of beat-to-beat QT (time interval between electrocardiographic Q and T waves) alternation (21), whose cellular counterpart is APD alternans and which can be originated from instability either in membrane voltage or in calcium cycling (22). Lemay et al. have proposed a procedure for predicting alternans based on randomly varying pacing protocols and on processing CL and APD sequences in the frequency domain (23). Along the same line, Prudat et al. have shown that rabbit ventricular myocytes are prone to calcium-driven, rather than voltage-driven, alternans (24), confirming what was found by Knaporyis and Blatter in ventricular, as well as in atrial, rabbit myocytes (25). A further method to compare pacing and AP repolarization variability is that of making pacing CL to alternate, which is clinically relevant because oscillation in heart rate has been observed in postmyocardial infarction and in hypertensive patients (26). By means of this approach, applied in computational and experimental recordings of transmembrane potential and intracellular calcium, Weinberg and Tung have shown that CL oscillations can promote either a proarrhythmic or an antiarrhythmic substrate, depending on whether APD and calcium alternans are locally (single-cell) or spatially (tissue) concordant or discordant (27,28).

In this study, I further explore the interplay between sER and btb-ER for sequences of APs simulated by means of O'Hara et al.'s human ventricular AP model (29), paced with stimulation protocols in which CL changes beat-to-beat according, in turn, to sinusoidal, saw-tooth, and random law. I focus on high pacing frequencies, with CL variability range covering values known to bring about APD alternans under constant pacing rate. I describe three qualitatively different types of btb-ER configurations, depending on the rate of CL variability, and associated with a different degree of APD stability, measured after a perturbation introduced by a premature beat. The morphology of btb-ER of an AP sequence under periodic pacing contains, therefore, relevant information on the dynamics of repolarization at high pacing rate, which can be extrapolated to the case of nonperiodic variability. A better knowledge of AP repolarization dynamics at high and highly variable pacing rate, particularly of parameters that can discriminate the degree of APD stability under pacing perturbations, can 1) contribute to explain the transition from abrupt heart rate acceleration to VF, which often accompanies sudden cardiac death (30), and 2) assist in evaluating complex effects on AP repolarization of antiarrhythmic treatments.

METHODS

All simulations presented in this study have been performed on the O'Hara et al. human ventricular AP model (OR; 29). The "ode15s" solver built into the R2018a version of Matlab (The MathWorks, Natick, MA) was used to integrate model equations. All simulations were run on a PC with Intel(R) Core (TM) i7, 2.8 GHz CPU. APs were elicited by simulating 0.5-ms-long current injections with an amplitude 50% above current threshold. AP duration was measured as $APD_{-60\ mV}$, i.e., the time between the maximal first derivative of membrane potential (V_m) during the initial fast depolarization phase and the time during repolarization when V_m reached the value of −60 mV. In some simulations, the amplitude of AP-driven intracellular calcium (Ca_i) transient was also measured by subtracting the initial value of $[Ca^{2+}]_i$ immediately before the stimulus current injection to its peak value reached during the AP.

sER

sER was measured in steady-state conditions by conditioning the membrane at a given basic CL (BCL), delivering an extra stimulus delayed within BCL ± 50 ms (step 5 ms), and reporting the resulting APD versus the variably delayed preceding CL.

Families of ERs

Standard sERs were also measured in dynamic conditions for each beat of an AP sequence. The vector of model variables was saved at the end of any given n^{th} beat and used instead of the constant pacing train to initialize the model before applying the sER pacing protocol. The measurement resembles that of a standard S1S2 restitution because it provides, for each beat, all next APD_n given any arbitrary CL_{n-1}. Each sER of an AP sequence is then related to a "state" identified by the couple (CL_{n-1}, APD_n).

btb-ER

btb-ER is defined here for AP sequences paced at variable pacing rate as the collection of the states of the sequence, i.e., APD of each beat versus the preceding CL.

Pacing protocols

AP sequences were obtained by making CL varying, in turn, like a sinus wave:

$$CL(N) = \mathrm{BCL} + \sigma \times \sin(\omega \times N), \tag{1}$$

with a saw-tooth law

$$\begin{aligned} CL(N) &= CL(N-1) + \mu \quad and\ \mu \\ &= -\mu \ \ when\ CL(N) reaches\ BCL \\ &- \sigma \ \ \mathrm{OR}\ when\ CL(N) reaches\ BCL + \sigma \end{aligned} \tag{2}$$

or randomly:

$$\begin{aligned} CL(N) &= CL(N-1) + \mu \times rand^{\pm} \ \ and\ \ BCL \\ &- \sigma < CL < BCL + \sigma, \end{aligned} \tag{3}$$

where N is the beat number, BCL the basic cycle length, σ the half range of CL variability, ω the frequency of CL oscillations, μ ($< \sigma$) a given constant increment of CL, and $rand^{\pm}$ a beat-to-beat randomly assigned sign.

RESULTS

Periodic pacing

I paced the OR model with a periodic pacing program according to Eq. 1, with BCL = 300 ms, σ = 50 ms, and ω = 0.6. Fig. 1 *A* shows, superimposed, the temporal sequence of CLs (*red curve*) and APDs (*black dots*). In Fig. 1 *B*, the corresponding btb-ER representation is shown, in which each APD of the sequence is reported as a function of the preceding CL. The range of CL variability includes values (~250–270 ms) at which APD alternans is expected at constant BCLs (Fig. 2). I repeated simulations like those in Fig. 1 for different values of ω, from 0.02 (number of beats $N_{0.02}$ required for a complete CL oscillation is 314, i.e., period $T_{0.02}$ ~1.6 min) up to 2.4 ($N_{2.4}$ = 2.6, i.e., $T_{2.4}$ ~0.8 s). Results for three ω-values are reported in Fig. 3. I found that, for ω-values lower than 0.04, btb-ER follows a unique curve that splits into two branches (Fig. 3 *A*, *red arrows*) for CL-values within the range of APD alternans (see Fig. 2). Transition to alternans during CL shortening occurs progressively earlier as ω decreases (see *green arrows* in *inset* of Fig. 3 *A*) until the btb-ER curve coincides with steady-state rate dependence of APD (RD_{APD}) as ω values approach zero. I denote this btb-ER behavior for $0 < \omega < 0.04$ as type 1. For $0.04 < \omega < 0.6$, I measure a different behavior (type 2), in which the decrease of CL into the 250–270 ms range does

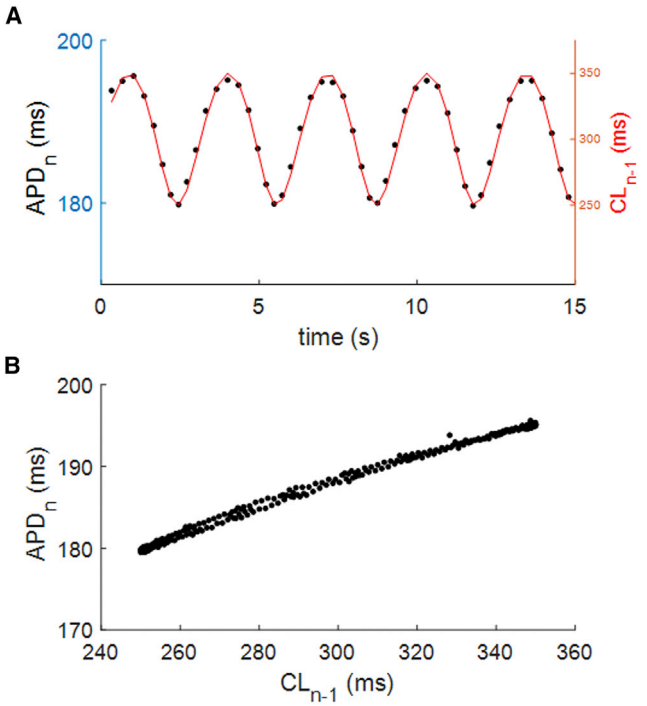

FIGURE 1 APD-CL phase and dynamic restitution. (*A*) A superimposed time course of APD_n (*blue*) and CL_{n-1} (*red*) of a sequence of consecutive APs, elicited periodically according to Eq. 1, is shown. (*B*) APD_n versus CL_{n-1} representation (btb-ER) of the same sequence is shown. To see this figure in color, go online.

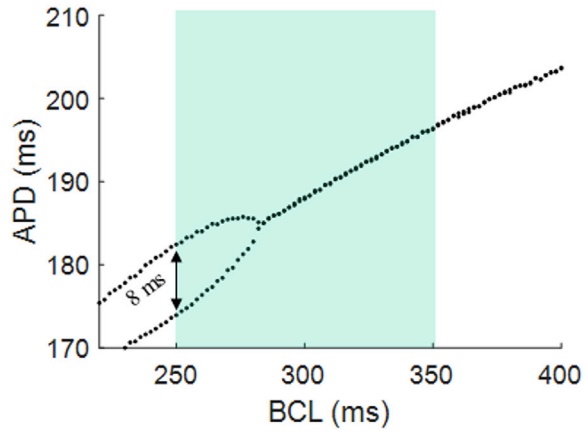

FIGURE 2 Steady-state rate dependence of APD. Steady-state APD values were measured at constant pacing rates and reported in the figure as a function of BCLs from 220 to 400 ms. CL-values below 280 ms lead to stable APD alternans (see also Figure 14 in (29)). To see this figure in color, go online.

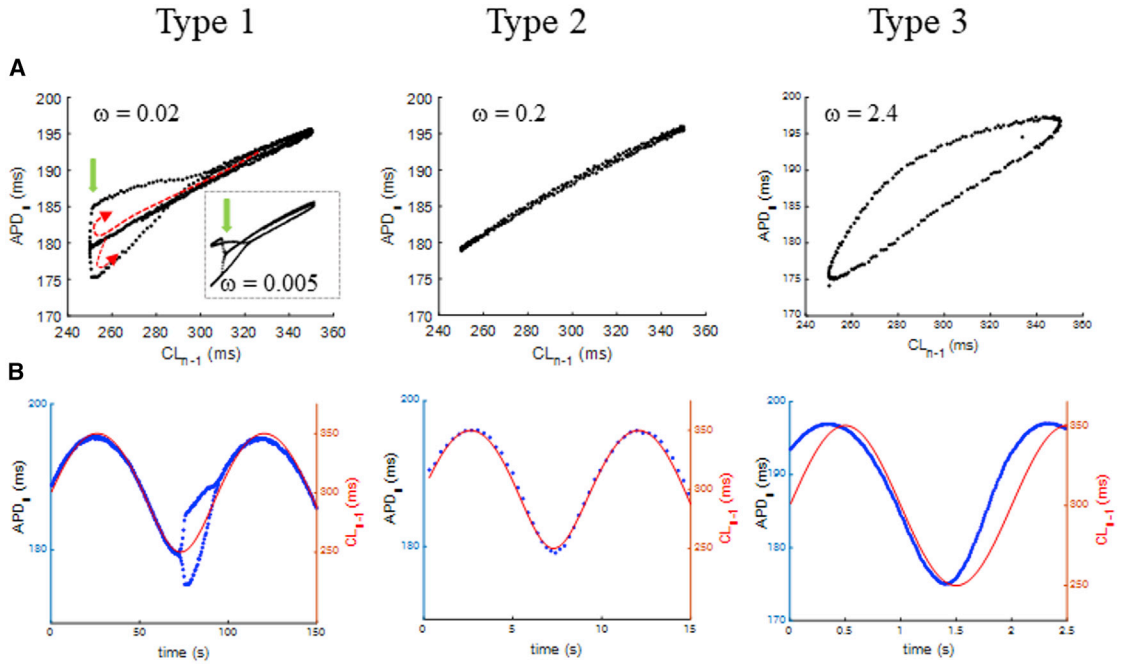

FIGURE 3 btb-ER and time course of APD and CL under sinusoidal pacing. Sequences of 500 APs were elicited with CL varying according to Eq. 1, with BCL = 300 ms, $\sigma = 50$ ms, and $\omega = 0.02$, 0.2, and 2.4 (*first*, *second*, and *third column*, respectively). (*A*) btb-ER representations of the sequences are shown in which each APD is reported as a function of the preceding CL. Inset in (*A*) shows additional btb-ERs measured at $\omega = 0.005$. (*B*) Time courses of CL_{n-1} (*red*) and APD_n (*blue*) are shown for the sequences reported in (*A*). To see this figure in color, go online.

not lead to alternans and the dynamic ER curve is a single curve, i.e., APD_n and CL_{n-1} oscillate in phase (Fig. 3 *B*, *middle panel*). Finally, for $0.6 < \omega < 2.4$, I find a behavior in which a variable phase shift between APD_n and CL_{n-1} develops (Fig. 3 *B*, *right panel*), which results in hysteresis in the btb-ER (type 3). The same three types of behavior were found with a pacing protocol in which CL changed according to a saw-tooth law Eq. 2), as shown in Fig. 4. The parameter controlling the transition from one type to another was, in this case, the μ value of Eq. 2.

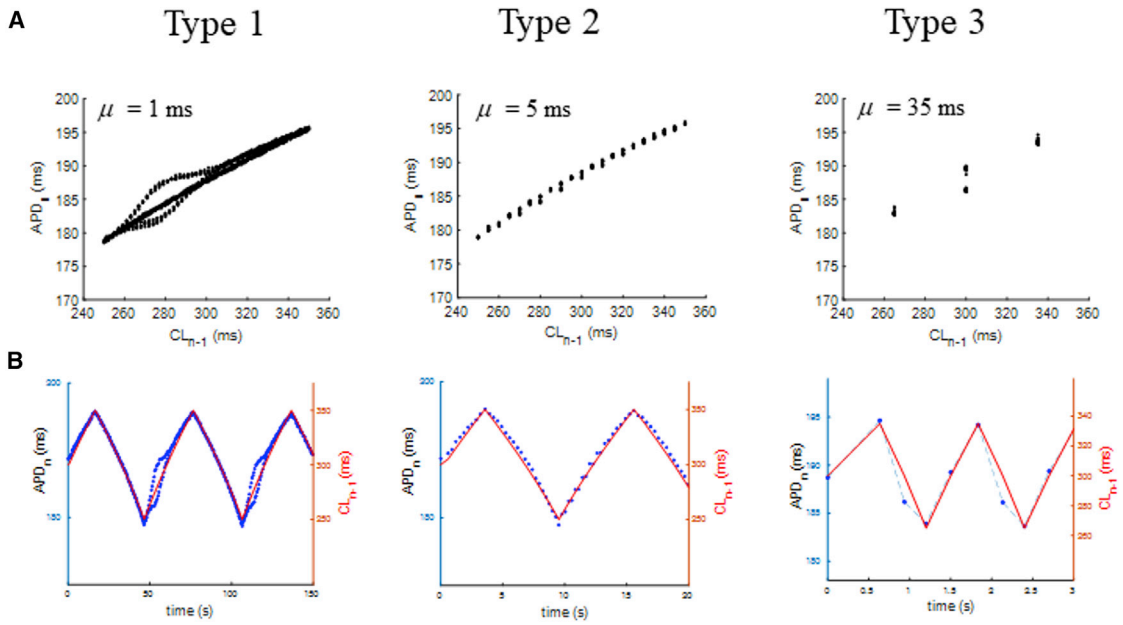

FIGURE 4 btb-ER and time course of APD and CL under saw-tooth pacing the same as in Fig. 3 for AP sequences elicited with CL varying according to a saw-tooth law (Eq. 2), with $\mu = 1$, 5, and 35 ms, respectively. To see this figure in color, go online. (*A*) btbER representations of the sequences; (*B*) time-courses of CLn-1 (*red*) and APDn (*blue*) for the sequences reported in (*A*).

Random pacing

The OR model was also paced with a protocol in which CL changed randomly from beat to beat according to Eq. 3, with the same BCL (300 ms) and the same range of CL variability (± 50 ms) used for periodic pacing. Different simulations were performed with different values for μ. Again, the three types of btb-ER behavior emerged, even though the difference in vertical spread of btb-ER between type 2 and 3 was less pronounced than in the periodic pacing (Fig. 5). Of course, the phase relationship between APD_n and CL_{n-1} cannot be shown in this case. The type of variability adopted here, a one-dimensional random walk of CL within BCL $\pm$ σ, has been used to keep μ constant over the entire CL range, as in saw-tooth pacing protocols, with no periodicity.

Families of sER curves

Another way to look at the same restitution behavior is through sER curves. For each beat of the AP sequences described in Figs. 3, 4, and 5, the corresponding sER curve was measured as explained in Methods and the resulting families of curves reported for the different pacing conditions in Fig. 6. In the case of periodic pacing, as expected from btb-ERs, the vertical displacement of sER families was always relatively large in type 1 sequences. Vertical displacement was reduced for type 2 sequences and again increased for type 3 (Fig. 6, *A* and *B*). In the case of random pacing, the vertical width of the family of sER curves slightly increased from types 1 and 2 and again increased in type 3. The thickness of families of sERs, reported as red numbers in the figure, was measured as the distance between the upper and the lower sERs of the family, measured at the BCL (see Eqs. 1, 2, and 3).

Ionic modulation of btb-ER behavior

To investigate the role of ion currents and intracellular ion dynamics in modulating the three types of btb-ER behavior described above, I separately analyzed the ω interval in which APD alternans takes place (type 1) and that of types 2 and 3 (Figs. 7, 8, and 9). Intracellular ion dynamics was studied by blocking sarcoplasmic reticulum (SR) calcium release (Fig. 7 *A*), blocking SR calcium release and uptake (Fig. 7 *B*), clamping $[Ca^{2+}]_i$ constant (Fig. 7 *C*), and clamping $[Na^{+}]_i$ constant (Fig. 7 *D*). The role of the main ion currents involved in AP repolarization was studied by 50% decreasing the maximal conductance of L-type calcium current I_{CaL} (Fig. 7 *E*), the transient outward potassium current I_{Kto} (Fig. 7 *F*), and slow delayed rectifier potassium current I_{Ks} (Fig. 7 *G*). In the case of the rapid delayed rectifier potassium current I_{Kr} (Fig. 7 *H*), a 50% decrease produced an AP prolongation not compatible with the high pacing rate, and a 25% decrease was applied. Results are reported as black dots, superimposed to control results in light red.

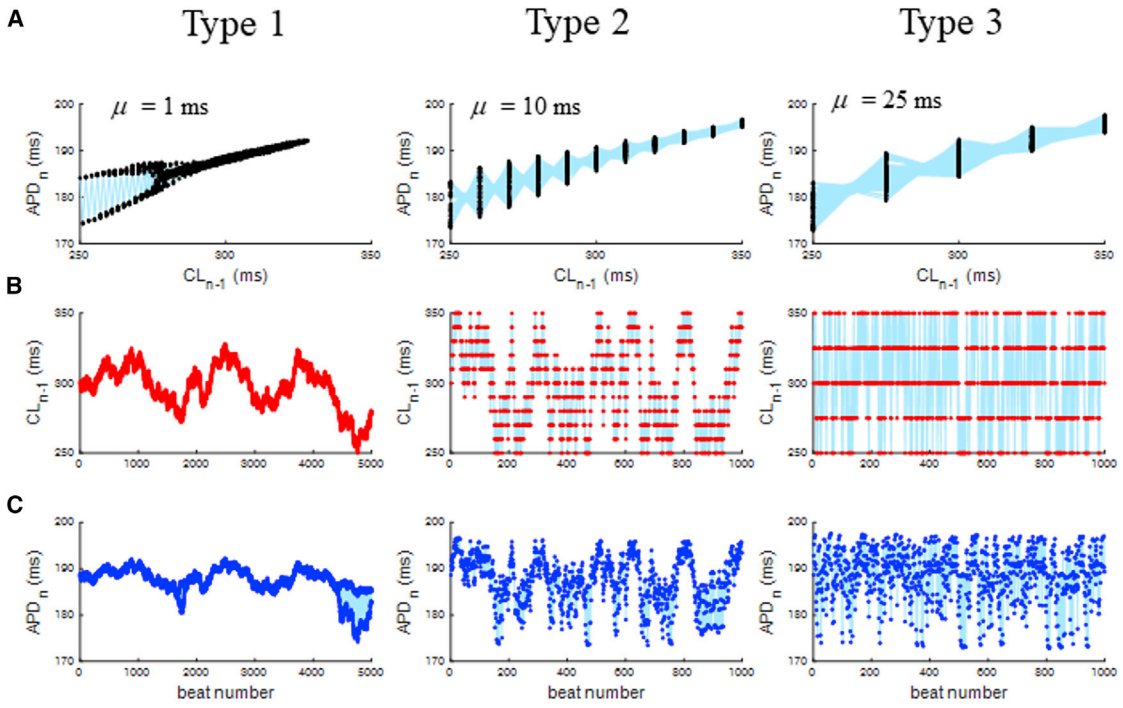

FIGURE 5 btb-ER and time course of APD and CL under random pacing the same as in Figs. 3 and 4 for AP sequences elicited with CL varying according to a random law (Eq. 3), with $\mu = 1$, 10, and 25 ms, respectively. (*B*) and (*C*) report, separately, CL and APD sequences that are superimposed in Figs. 3 and 4 *B*. Successive CL and APD data points are connected with light blue lines to better appreciate variations on a beat-to-beat basis. To see this figure in color, go online.

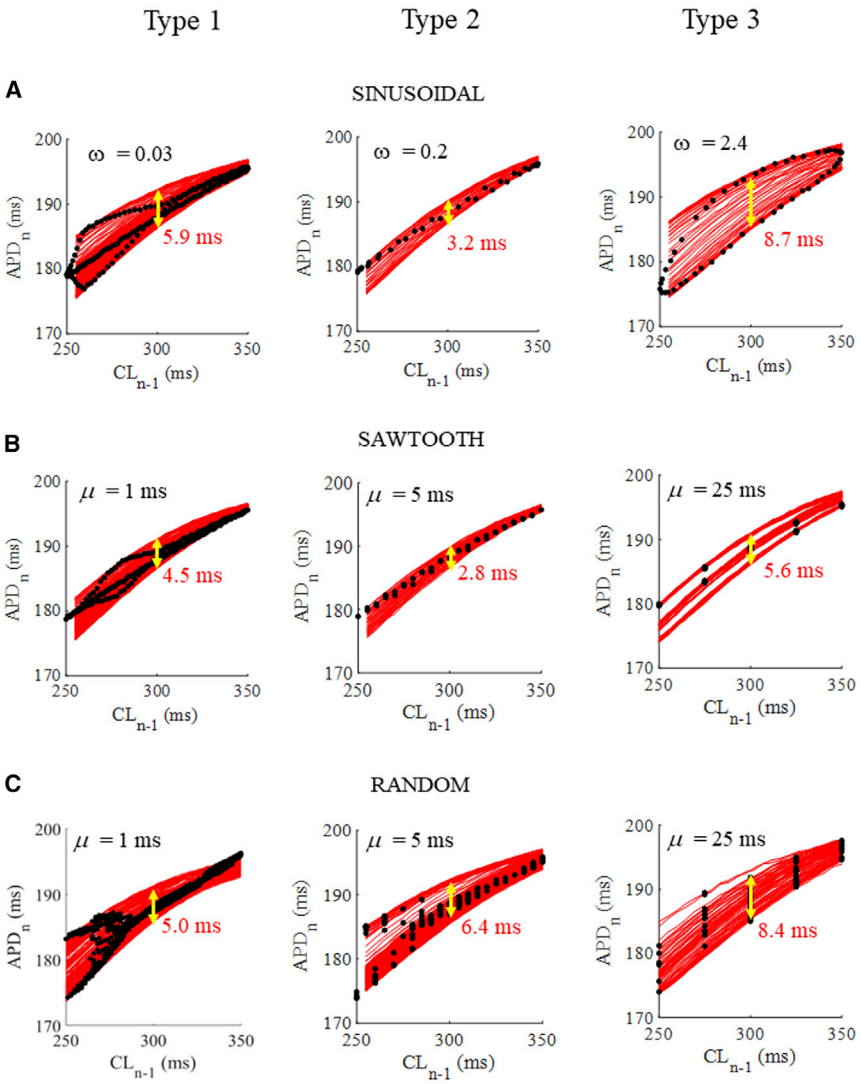

FIGURE 6 The family of sERs for an AP sequence. btb-ER representations (*black dots*) are reported in figure for the three types of pacing (*A–C*, respectively), corresponding to slow, intermediate, and fast beat-to-beat CL changes (*columns 1*, *2*, and *3*, respectively). For each state of each sequence, the corresponding sER curve (*red curves*) was measured and superimposed to the btb-ERs. Yellow double arrows and red numbers indicate the vertical width of each sER family. To see this figure in color, go online.

Type 1 behavior

Fig. 7, *A–D* show that intracellular calcium and sodium transients play a major role in controlling the transition to APD alternans at high pacing rate for ω-values (reported at the *bottom*) generating type 1 behavior. The removal of SR calcium release (Fig. 7 *A*), the complete exclusion of the SR from calcium cycling (Fig. 7 *B*), and the complete block of calcium dynamics (Fig. 7 *C*) remove the transition to APD alternans without affecting AP duration. Moreover, Fig. 8 shows that as the amount of calcium released from the SR progressively decreases, the CL window leading to APD alternans does also until alternans is completely removed when SR release is blocked (Fig. 7 *A*). Fig. 7, *E–H* show that the partial block of the main ion currents involved in AP repolarization only slightly modify conditions and extent of APD alternans, even when considerable changes in APD are introduced. Only under 50% reduction of G_{CaL} does the extent of APD alternans decrease, and alternans requires ω-values smaller than 0.02 to appear.

Type 2 and 3 behavior

Because the appearance of hysteresis in the btb-ER representations is due to differences in the phase relationship between APD and CL, I study this relationship in more detail for an ω interval between 0.1 and 2.4 (step 0.1) and see how modulation of intracellular ion dynamics and transmembrane ion currents described above affect this property. Beat-to-beat periodic pacing conditions are the same described for simulations of Fig. 3. Fig. 9 *A* shows the procedure used to measure the difference in the CL-APD phase relationship between pacing conditions where CL is increasing and decreasing within BCL $\pm$ σ. The top panels show three examples of APD_n (*red*) and CL_{n-1} (*black*) sequences of the same types reported in Fig. 3 *B*, for three increasing ω values. Hilbert transforms were used here to

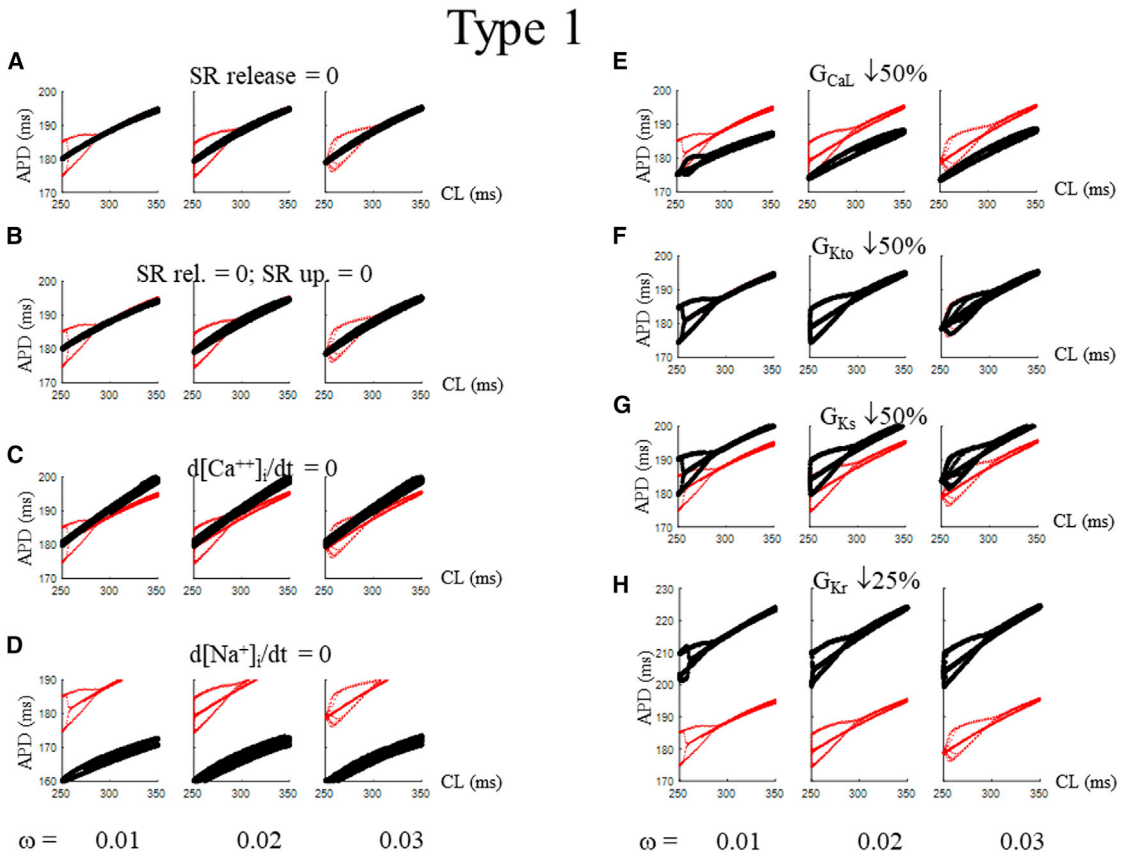

FIGURE 7 Modulation of bistability in type 1 responses. Simulations like those of Fig. 3 were repeated in more detail in the ω range 0.01–0.10, step 0.01 (only 0.01–0.03 are reported in figure), in control conditions (*light red*) and under application of the following treatments: (*A*) complete block of SR calcium release, (*B*) complete block of SR calcium release and uptake, (*C*) buffering intracellular calcium at its telediastolic value, (*D*) buffering intracellular sodium at 11.41 mM, (*E*) 50% reduction of maximal G_{CaL}, (*F*) 50% reduction of maximal GK_{to}, (*G*) 50% reduction of maximal G_{Ks}, and (*H*) 25% reduction of maximal G_{Kr}. To see this figure in color, go online.

calculate the instantaneous phase of the two discrete CL and APD sequences (31,32). ϕ_{APD} is the absolute value of the phase difference between the two,

$$\phi_{APD,CL} = |H(CL_{n-1}) - H(APD_n)|, \quad (4)$$

and is reported as a blue curve in the lower panels of Fig. 9 *A*. A_{up} and A_{down} are the areas under the CL-increasing and CL-decreasing portion of the two curves over one cycle of CL oscillation; thus, $A_{up} - A_{down}$ measures the asymmetry in the hysteretic btb-ER_{CL}

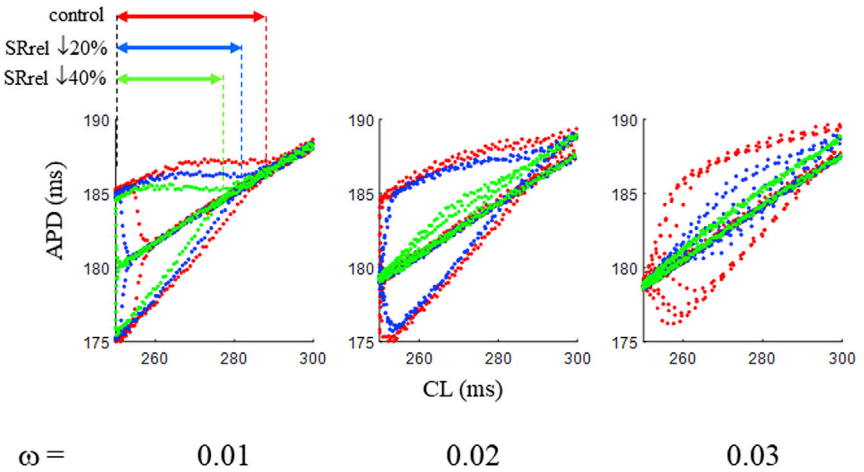

FIGURE 8 SR release and bistability in type 1 responses. Simulations like those in Fig. 7 were repeated, with progressive reduction of SR calcium release of 0% (*red*, control), to 20% (*blue*) and 40% (*green*). As SR release decreases, so does the CL interval (double arrows on the *top* of *first panel*) at which APD alternans takes place. To see this figure in color, go online.

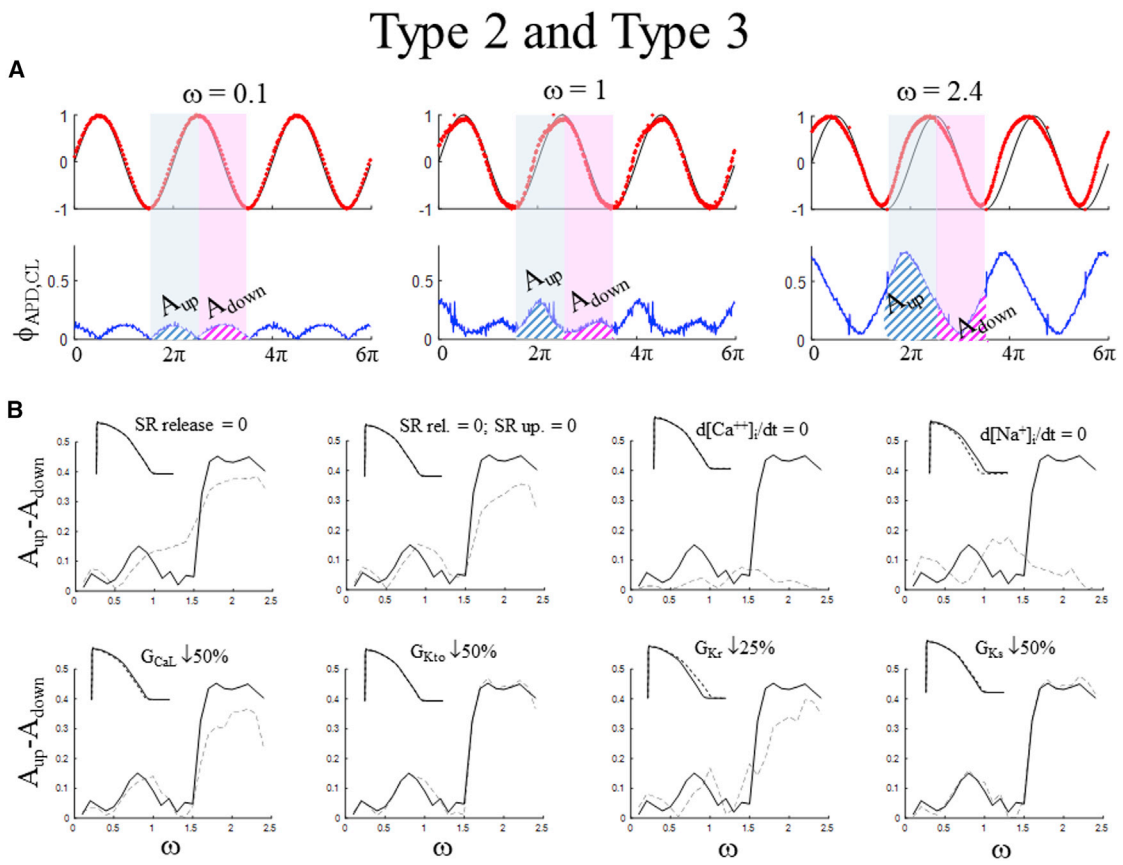

FIGURE 9 Modulation of CL-APD phase shift in type 2 and 3 responses. (*A*) Top shows superimposed normalized CL (*black*) and APD (*red*) sequences simulated by the pacing protocol of Eq. 1 (BCL = 300 ms, $\sigma = 50$ ms) for three different ω-values (reported in figure). Bottom shows absolute value of the phase difference (*blue*) between CL and APD as measured with Hilbert transforms (see text). ϕ_{up} is the area of the Δphase when CL is increasing (*gray shaded area*) and ϕ_{down} that when CL is decreasing (*pink shaded area*). (*B*) $\phi_{up} - \phi_{down}$ measures the phase asymmetry evident in the hysteretic behavior of btb-ERs and is reported (*broken lines*) in the ω range 0.1–2.4, step 0.1 (type 2 and 3 responses), for each of the treatments described in Fig. 7, superimposed to the same measure in control conditions (*solid lines*). To see this figure in color, go online.

representations, like those reported in Fig. 3 *A*. This quantity is reported in Fig. 9 *B* for control conditions (*solid line*) and for the same eight treatments of Fig. 7 (*broken lines*) as a function of the ω-value controlling the rate of beat-to-beat CL changes. CL-APD phase difference increases overall in control as ω does, with a small peak at $\omega = 0.8$ and a large band for $1.5 < \omega < 2.4$. Small $A_{up} - A_{down}$ values correspond to type 2 responses, whereas large values correspond to type 3. Ion-channel modulation and the exclusion of SR from calcium cycling only slightly affect the CL-APD phase, whereas separately, intracellular calcium and sodium buffering almost completely abolish phase asymmetry.

From the same simulations of Fig. 9 *A*, the time course of the peak of intracellular calcium transient (Cai_n) was also measured and reported in Fig. 10 *A*, superimposed in green with that of CL_{n-1} (*black*), and of APD_n (*red*). Phase difference between APD_n and Cai_n was measured as in Eq. 4 and reported (*blue curve*) in the bottom panels of Fig. 10 *A*. $A(\phi_{APD,Cai})$ is the area under this curve over one cycle of CL oscillation (*shaded*). Fig. 10 *B* shows that the phase shift between APD and Ca_i increases in control conditions as ω does. This behavior is almost insensitive to changes in maximal conductance of ion currents (data not shown) but does depend on interventions affecting intracellular calcium dynamics such as block of SR calcium release (*sparsely dotted line*) or buffering intracellular sodium (*densely dotted line*).

Stability of AP repolarization

I have defined as state of a beat the couple of values (CL_{n-1}, APD_n). An AP sequence is a series of states; a btb-ER the graphic representation of these states. I introduce an arbitrary working definition of repolarization stability of a state when it is perturbed, i.e., with CL_{n-1} anticipated of 50 ms. Instability is the number of beats taken for APD_n to recover its unperturbed time course after the premature beat. Other types of perturbation could be applied as a missing beat (16) or any variably delayed pre- or postmature stimulus, with qualitatively similar results. Fig. 11 shows schematically the protocol, applied to an AP sequence periodically paced according to Eq. 1 (CL = 300 ms, $\sigma = 50$ ms,

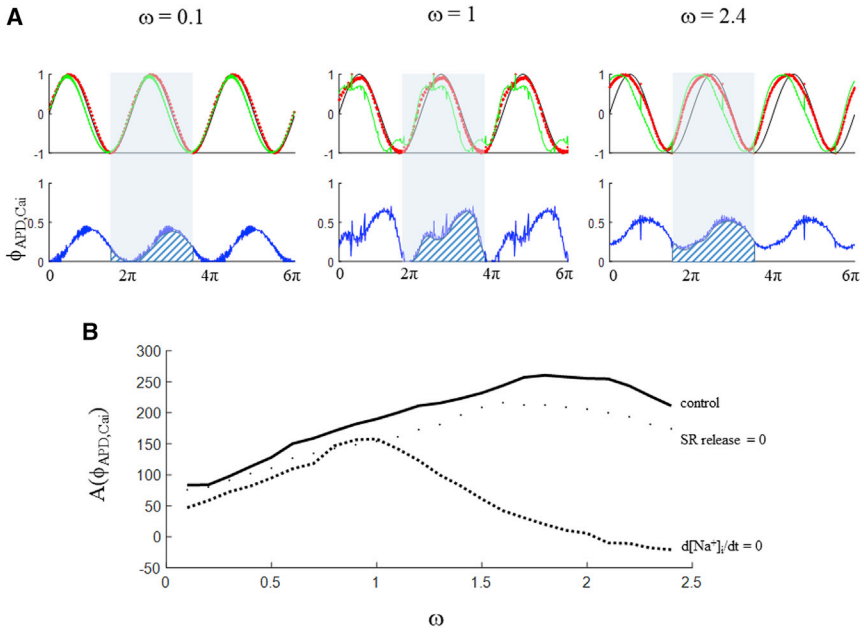

FIGURE 10 APD-Ca_i phase shift. (*A*) Top shows superimposed normalized CL (*black*), APD (*red*), and Ca_i (*green*) sequences simulated by pacing protocol of Eq. 1 (BCL = 300 ms, $\sigma = 50$ ms) for three different ω-values (reported in figure). Bottom shows phase difference (*blue*) between APD and Ca_i as measured with Hilbert transforms (see text). (*B*) $A(\phi_{APD,Cai})$ is the area under the blue curve of (*A*) for one cycle of CL oscillation, measured in control conditions (*solid line*), under complete block of SR calcium release (sparsely *dotted line*), and by clamping $[Na^+]_i$ constant (*densely dotted line*). To see this figure in color, go online.

$\omega = 0.6$). Under these pacing conditions, APDs oscillates in phase with CL following a sinusoidal law, shown by the blue dots in Fig. 11 *B*. When the CL indicated by the blue arrow in Fig. 11 *A* is made 50 ms shorter (*red dot*), APDs deviate from the control values for a given number of beats (*red dots*). The absolute value of the difference between control and perturbed values (ΔAPD) is reported in Fig. 11 *C*. I quantify instability as the area under the curve ΔAPD versus the number of beats N (arbitrarily chosen <30). This parameter will be different depending on which beat of the sequence has been prematurely stimulated. Taking the absolute value of the APD difference removes the possibility of discriminating between perturbation-induced alternating and nonalternating APD changes with respect to the unperturbed APD sequence. It should be noted, however, that APD changes, with only a few exceptions in the first two beats after perturbation, were alternating in all instances.

In Fig. 12 *A*, I show the application of the protocol described above for each of the 200 beats of AP sequences, sinusoidally paced with CL = 300 ms, $\sigma = 50$ ms, and six different ω-values. For each beat, CL was anticipated by 50 ms and the corresponding ΔAPD (N) measured. The top panels show three examples in which the anticipated beat occurred at CL ~250 (*black*), CL ~300 (*red*), and CL ~350 (*blue*). The bottom panels show all ΔAPD(N) curves along the z axis in a color code (see *color bar*) as a function of beat number and of the anticipated CL value. The yellow horizontal band in the lower part of the first bottom panel shows that for very low rate of beat-to-beat CL changes ($\omega = 0.02$), the premature beat triggers a quasi-steady-state oscillation of APD around the unperturbed APD sequence (see *black* and *red traces* in *top panel*), the same amplitude of the APD alternans found in steady-state conditions (see Fig. 2). As ω increases, alternans is progressively removed, at first in a complex V-like shape, where perturbations for CL-values close to 350 ms show a fast early recovery, followed by a later re-increase in ΔAPD (*blue curve* in *second top panel*) and then a homogeneous decrease for all CL values. In Fig. 12 *B*, the same measurements were performed on sequences paced with saw-tooth varying CL (Eq. 2), with CL = 300 ms, $\sigma = 50$ ms, and six different μ values, with similar results. Same simulations were performed on randomly paced sequences and reported in Fig. 12 *C*. To cover the entire range of CL variability, I run in this case 5 sequences of 20,000 beats like those reported in Fig. 5 *C*, and I extracted a total sample of 3000 beats, on which I performed the analysis reported in Fig. 12 *C*. Whereas the area under ΔAPD curves measures the stability of the corresponding beat, the volume underlying the color surfaces reported in bottom panels of Fig. 12 represents an estimate of the stability of an entire AP sequence at the corresponding pacing conditions (CL, ω, σ, and μ). This stability parameter is reported in Fig. 13 in the case of sinusoidal pacing as a function of ω and, in the case of saw-tooth or random pacing, as a function of μ.

DISCUSSION

Heart rate variability (HRV) has a very complex frequency distribution with a high-frequency component mainly mediated by vagal activity and by the respiratory cycle (33). The latter, known as respiratory sinus arrhythmia,

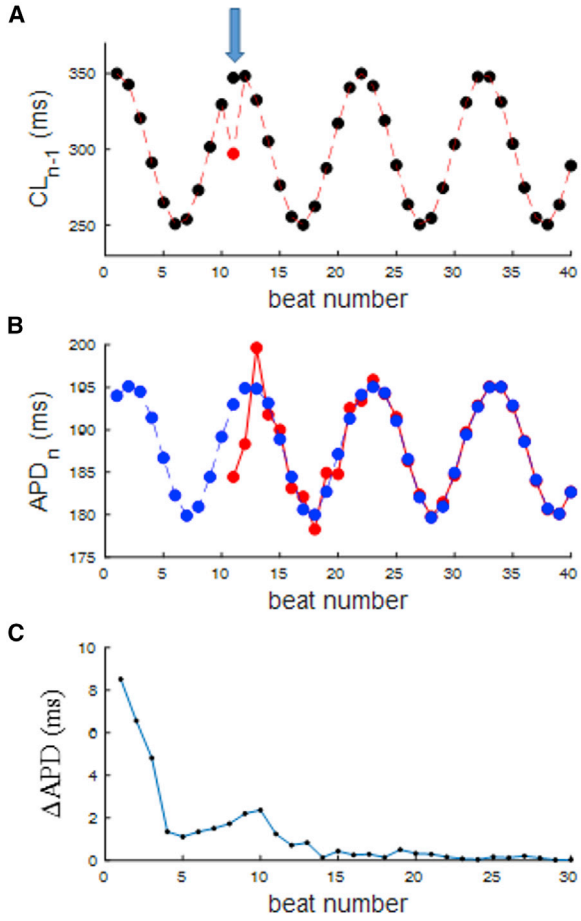

FIGURE 11 Stability of a state. (*A*) Black dots represent a pacing train with CL varying sinusoidally according to Eq. 1 (BCL = 300 ms, σ = 50 ms, ω = 0.6). (*B*) Corresponding APDs (*blue dots*) after each CL in (*A*) are shown. The simulation was repeated by anticipating a CL value of 50 ms (*arrow* and *red dot* in *A*) and the deviations of APD from the unperturbed AP sequence reported in (*B*) as red dots. (*C*) shows the absolute value of the difference between perturbed and unperturbed sequences in (*B*) as a function of number of beats after the premature stimulus. I take the area under this curve as an inverse measure of the stability of the corresponding state. To see this figure in color, go online.

introduces RR (time interval between two consecutive electrocardiographic R waves) oscillations around 0.3–0.4 Hz in a resting subject, which can increase as the cardiorespiratory activity does and, interestingly, disappear in pathological conditions like heart failure, leading to a substrate more prone to arrhythmias (33,34). A large part of the HRV frequency spectrum is stochastic, and a decrease in this component, mainly attributed to autonomic nervous system tone damage, is a known predictor for arrhythmia (35). Despite the large body of clinical evidence of the proarrhythmic outcome of low RR variability in cardiac electrocardiographic signal (ECG), the underlying cellular dynamics of the phenomenon is far to be established.

The aim of this computational study is to investigate the dynamics of APD variability at high pacing rate and under different types (sinusoidally, saw-tooth, and randomly variable) and extent of beat-to-beat CL variability. The significance of exploring these three types of activation protocols is double. The first aim is to qualitatively classify AP dynamics under different types of physiopathological variability in pacing CL by controlling parameters of this variability. Because we cannot expect real in vivo CL changes that follow a saw-tooth regimen, nevertheless—and this is the second aim of the study—I want to show that features such as short-term AP memory or a protective role against AP repolarization instability are common to different types of pacing variability and depend on pacing parameters that can be controlled experimentally. In the range of pacing rate under study, three types of behavior emerge, which can be visualized in three qualitatively different btb-ER forms that are associated with different degrees of APD stability. The range of CL variability explored (in *green* in Fig. 2) goes from 250 to 350 ms and includes values (<280 ms) at which 8-ms-wide APD alternans occurs in steady-state pacing conditions in the O'Hara model (29), and in agreement with experimental data on undiseased human ventricular myocytes (36).

Type 1 responses

Type 1 behavior (*left panels* of Figs. 3 *A*, 4 *A*, and 5 *A*) is characterized by a btb-ER form qualitatively similar with the RD_{APD} curve (Fig. 2) and emerges when the pacing CL range is spanned with low values of beat-to-beat CL changes ($\omega < 0.04$ under sinusoidal pacing, $\mu < 3$ ms under saw-tooth or random pacing). AP repolarization tends to be unstable when states with CL-values in the lower range of variability are perturbed by shortening their CL by 50 ms. The AP instability of these pacing conditions (*first columns* of Figs. 12 and 13) is due to the Hopf bifurcation that characterizes the steady-state RD_{APD} curve. A premature beat, like the one that I adopt to perturb pacing, easily triggers APD alternans, as is shown from the yellow horizontal band in the left panels of Fig. 12. Thus, low beat-to-beat CL changes at high pacing rate can trigger APD alternans, which is known to precipitate conditions leading to VF in the heart (27,28). Membrane ion currents involved in AP repolarization, despite their prolonging-shortening effect on APD, have only a small modulatory effect on the extent and dynamics of APD alternans under these pacing conditions (Fig. 7, *E–H*). Moreover, the results obtained by reducing or removing calcium transient (Fig. 7, *A–C*) suggest that APD alternans, at high pacing rate and for low rate of beat-to-beat CL changes, is mostly calcium-driven, as already observed recently by Prudat et al. (24). The greater effect found in ion current modulation is that of reduction of G_{CaL}, likely because of its linking action between membrane current and calcium dynamics. Intracellular sodium concentration has been

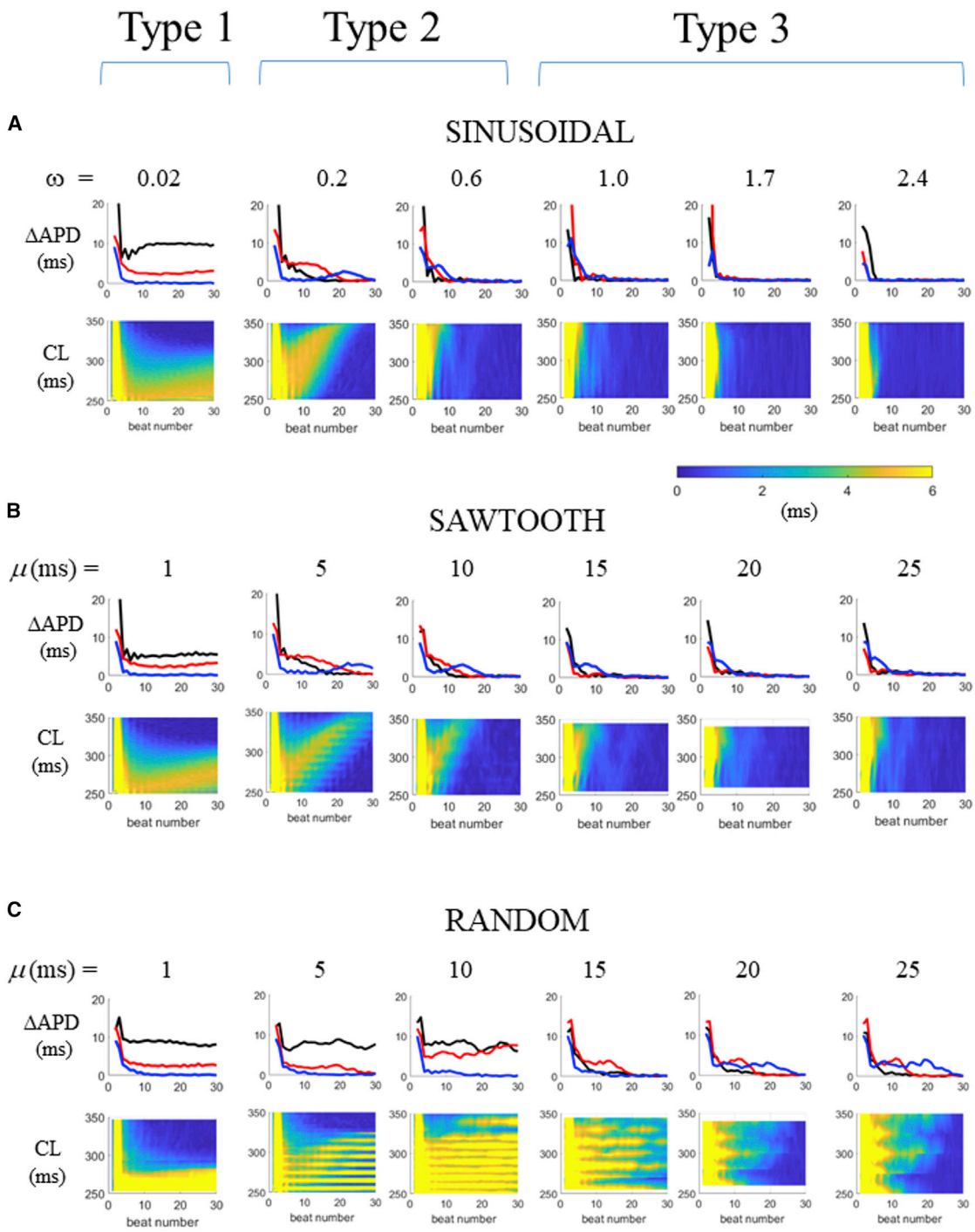

FIGURE 12 Stability of beats and sequences. The stability protocol shown in Fig. 11 was applied in AP sequences obtained under sinusoidal (*A*), saw-tooth (*B*), and random (*C*) pacing and for different values of beat-to-beat CL changes (ω- and μ-values reported in figure). Each panel reports on the top three colored curves such as those in Fig. 11 *C* obtained by anticipating CL in states with unperturbed CL ~250 ms (*black*), ~300 ms (*red*), and ~350 ms (*blue*). These ΔAPD curves were measured for each beat of each AP sequence and reported along the z axis in color code (see *color bar*) as a function of perturbed CL and beat number in the bottom part of each panel. I take the volume under these surfaces as an inverse measure of the overall stability of the corresponding AP sequence. To see this figure in color, go online.

thought of as a memory variable by Schaeffer et al. (19), who found that clamping it constant shortens APD and partially remove AP memory properties. Simulations of Fig. 7 *D* confirm APD shortening, even though the effect on short-term AP memory does not appear in type 1 responses as we will see it in type 2 and 3.

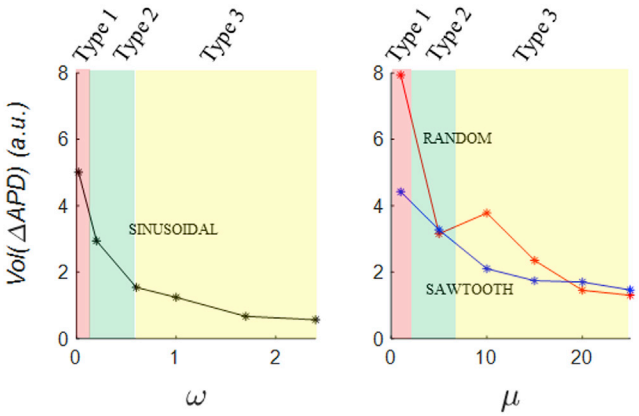

FIGURE 13 Stability of sequences. The instability of AP sequences, measured as explained in Fig. 12, is represented in the case of sinusoidal pacing (*left*) as the volume under ΔAPD surfaces versus ω (*black*) and, in the case of saw-tooth and random pacing (*right*), as a function of μ (respectively, *blue* and *red*). Color shaded areas mark the ω and μ ranges corresponding to the three types of responses described (see Results). To see this figure in color, go online.

Type 2 and type 3 responses

In type 2 responses, btb-ERs modify their form in a single curve under periodic pacing (*central panels* in Figs. 3 *A* and 4 *A*) and in a thin scatter plot under random pacing (*central panel* in Fig. 5 *A*). Instability in AP repolarization affects the all-CL range with a biphasic ΔAPD behavior (early recovery and secondary transient increase, Fig. 12, *second* and *third columns*). Under these conditions, as the extent of beat-to-beat CL changes increases, the bistable effect of quasistationary pacing (type 1) decreases and AP repolarization stability increases (Fig. 12, *second* and *third columns*, and Fig. 13). Type 3 responses show a vertical growth of their btb-ERs, which take the form of hysteresis in the case of periodic pacing (Figs. 3 and 4). APD instability tends to be equally distributed along the entire CL range and decreases overall with the increase of ω and μ. Decreased repolarization instability is accompanied, in this case, with vertical spread of sERs measured along the AP sequence, which results in complexity of the btb-ER form and can be quantified under periodic pacing by analyzing the CL-APD phase relationship when the beat-to-beat rate of CL changes (ω) increases.

The lack of APD alternans under type 2 and type 3 conditions allows for performing the analysis of the phase relationship between CL and APD over the corresponding entire range of ω-values (Fig. 9), as another way to look at the transition between the two (see Fig. 3). The asymmetry in the CL-APD phase shift, also evident in the hysteretic form of btb-ER, grows in control conditions as ω does. Also, in this case, as seen for type 1 behavior, the phenomenon appears to be primarily due to calcium cycling rather than to membrane currents because the more relevant effect of ion-current modulation is the 50% reduction of I_{CaL}, supposedly because of its linking role between calcium cycle and membrane excitability. I speculate that CL-APD phase relationship is due to the interaction of intrinsically slightly phase-shifted calcium- and AP-dynamics oscillations, electrogenically coupled mainly by I_{CaL} and I_{NaCa}. Coupling becomes manifest when the AP cycle is driven periodically (with either a sinus wave or a saw-tooth CL waveform). When the calcium dynamics is abolished (by clamping $[Ca^{2+}]_i$ constant), only the membrane current process remains, and accordingly, CL-APD phase difference disappears. Simulations reported in Fig. 10 corroborate this speculation in the case of reduction of intracellular calcium dynamics by means of clamping $[Na^{+}]_i$ constant. This maneuver has the effect of decreasing the phase difference between APD_n and Cai_n, particularly for high ω values (Fig. 10 *B*), and, in turn, according to the above speculation, the phase asymmetry between APD_n and CL_{n-1} (Fig. 9 *B*, *fourth top panel*). Of course, the maneuver of clamping $[Ca^{2+}]_i$ constant abolishes the calcium transient and therefore could not be adopted to test the same hypothesis.

Other authors have focused on the phase relationship between APD and the intracellular calcium cycle to isolate conditions when the two are in—or out of—phase (22,27). The role of the intracellular sodium transient in generating short-term AP memory (19,37) and in allowing the antiarrhythmic effect of stochastic pacing (20) has been shown previously. In the simulation in which I clamp intracellular sodium constant, I adopt the same value (11.41 mM) that Dvir and Zlochiver (20) have used on the ten Tusscher and Panfilov (17) human ventricular AP model to show its direct link to the antiarrhythmic effect of stochastic pacing. As mentioned above, simulations shown for type 2 and 3 responses in Fig. 9 *B* support the finding of Schaeffer et al. (19) that intracellular sodium transients are involved in short-term AP memory, moreover, suggesting that this effect becomes significant only for large ω-values.

CL-APD phase shift and short-term AP memory

The study of the CL-APD phase relationship under periodic pacing makes it easier to display and measure a beat-to-beat feature of AP dynamics that is also shared by stochastic pacing, is ultimately described by the vertical spread of sER curves, and is associated with stability of AP repolarization. I have described previously that vertical dispersion of sER_{CL} curves measured during an AP sequence paced with beat-to-beat variable CL is an estimate of short-term AP memory, in the sense that the state of each beat does not belong to the sER measured at the corresponding time, i.e., the following activation interval (CL_{n-1}) does not uniquely identify the next APD (APD_n). Thus, the dynamics of the next beat, e.g., its APD, depends not only on the previous but on a certain number of preceding beats, which is the definition of short-term AP memory. Other authors have quantified this property by means of stability analysis with autoregressive stochastic modeling (20,23). The increase in the vertical

distance between individual sER curves with the increase of interbeat CL changes has been described previously (38) on APD_n versus DI_{n-1} representations and without reference to repolarization stability.

Also, hysteresis and a scattered appearance in btb-ER under sinusoidal or random pacing has been described (39,40), though under quite different conditions, in which pacing variability was driven by controlling on a beat-to-beat basis the DI instead of CL. Moreover, in that context, ER was reported as btb-ER_{DI} instead of btb-ER_{CL} as in this study. I have already discussed these differences elsewhere (16). What I want to emphasize here is the role of beat-to-beat CL changes in making AP repolarization more stable and that this role can be effectively monitored through the measure of btb-ER, whose shape and size is determined by the vertical spread of the family of sER curves recorded from each beat.

The three types of behavior described above suggest that beat-to-beat CL variability at high pacing rate can either bring about APD alternans or increase AP stability, depending on the rate of CL changes. The ability of CL oscillations to either promote proarrhythmic and antiarrhythmic substrates has been previously shown by Weinberg and Tung (27) and attributed to different couplings of APD and calcium transient oscillations. I demonstrate here that intracellular calcium dynamics controls both instability at low rate of CL variability and increased stability at high rate. In this latter case, stability is due to an increased level of short-term AP memory, which can be measured from the shape of btb-ER or from the analysis of the CL-APD phase shift. It has been suggested that, given the stabilizing role of beat-to-beat stochastic pacing variability on cardiac repolarization, a preset HRV can be added on artificial pacemaker function to reduce susceptibility to arrhythmias (41). This study suggests that sinusoidal pacing might be more efficient (see Fig. 13) in making AP repolarization more stable and should therefore be further explored in this sense.

Limitations

All simulations of this study were performed on the O'Hara et al. (29) AP model in its zero-dimensional (cellular) endocardial version. Thus, it does not take into account possible modulation of restitution and stability properties due to intrinsic transmural differences in AP waveform, as well as to intercellular electrical coupling. In addition, even though the range of pacing CLs explored is, particularly for values $\leq$300 ms, closer to those found for ventricular tachycardia rather than to a physiological sinus rhythm (36), it is nevertheless my main goal to investigate restitution dynamics within the range of pacing rates at which transition between the two states occurs. Finally, not all the tested pacing protocols could be suitably applied to animals or humans; the few minutes required for sinusoidal pacing at $\omega = 0.02$, for instance, can hardly be thought of in clinical practice but can be profitably applied in a number of experimental preparations.

CONCLUSION

The numerical simulations presented in this study, particularly those in Fig. 6, explain btb-ER morphology in terms of families of sER curves and would be nearly impossible to test in vivo in this much detail and in these terms. The approach, though, can be reduced to the simple analysis of btb-ERs, particularly their vertical displacement, after different types and extent of beat-to-beat CL variability. Because btb-ERs only require a beat-to-beat estimate of activation interval (CL or electrocardiographic RR) and duration of repolarization (APD and electrocardiographic QT), they can be suitable not only for transmembrane signals but also for any epicardial or ECG recording of cardiac electrical activity. Despite the limitations listed above, the procedure shows potentiality for monitoring short-term cardiac memory and repolarization stability in experimental and clinical research and provides a novel, to my knowledge, synthetic biomarker for testing effects of antiarrhythmic therapies on cardiac repolarization.

REFERENCES

1. Zaniboni, M., A. E. Pollard, …, K. W. Spitzer. 2000. Beat-to-beat repolarization variability in ventricular myocytes and its suppression by electrical coupling. *Am. J. Physiol. Heart Circ. Physiol.* 278:H677–H687.
2. Armoundas, A. A., M. Osaka, …, R. J. Cohen. 1998. T-wave alternans and dispersion of the QT interval as risk stratification markers in patients susceptible to sustained ventricular arrhythmias. *Am. J. Cardiol.* 82:1127–1129, A9.
3. Stein, P. K., and R. E. Kleiger. 1999. Insights from the study of heart rate variability. *Annu. Rev. Med.* 50:249–261.
4. Zaniboni, M., F. Cacciani, and N. Salvarani. 2007. Temporal variability of repolarization in rat ventricular myocytes paced with time-varying frequencies. *Exp. Physiol.* 92:859–869.
5. Gelzer, A. R., M. L. Koller, …, R. F. Gilmour, Jr. 2008. Dynamic mechanism for initiation of ventricular fibrillation in vivo. *Circulation.* 118:1123–1129.
6. Boyett, M. R., and B. R. Jewell. 1980. Analysis of the effects of changes in rate and rhythm upon electrical activity in the heart. *Prog. Biophys. Mol. Biol.* 36:1–52.
7. Choi, B. R., T. Liu, and G. Salama. 2004. Adaptation of cardiac action potential durations to stimulation history with random diastolic intervals. *J. Cardiovasc. Electrophysiol.* 15:1188–1197.
8. Fossa, A. A. 2017. Beat-to-beat ECG restitution: a review and proposal for a new biomarker to assess cardiac stress and ventricular tachyarrhythmia vulnerability. *Ann. Noninvasive Electrocardiol.* 22:e12460.
9. Garfinkel, A., Y. H. Kim, …, P. S. Chen. 2000. Preventing ventricular fibrillation by flattening cardiac restitution. *Proc. Natl. Acad. Sci. USA.* 97:6061–6066.
10. Franz, M. R. 2003. The electrical restitution curve revisited: steep or flat slope-which is better? *J. Cardiovasc. Electrophysiol.* 14 (*Suppl*):S140–S147.
11. Orini, M., J. Yanni, …, P. D. Lambiase. 2019. Mechanistic insights from targeted molecular profiling of repolarization alternans in the intact human heart. *Europace.* 21:981–989.

12. Osaka, T., E. Yokoyama, …, I. Kodama. 2011. Effects of chronic amiodarone on the electrical restitution in the human ventricle with reference to its antiarrhythmic efficacy. *J. Cardiovasc. Electrophysiol.* 22:669–676.
13. Koller, M. L., M. L. Riccio, and R. F. Gilmour, Jr. 1998. Dynamic restitution of action potential duration during electrical alternans and ventricular fibrillation. *Am. J. Physiol.* 275:H1635–H1642.
14. Osadchii, O. E. 2019. Effects of antiarrhythmics on the electrical restitution in perfused Guinea-pig heart are critically determined by the applied cardiac pacing protocol. *Exp. Physiol.* 104:490–504.
15. Goldhaber, J. I., L. H. Xie, …, J. N. Weiss. 2005. Action potential duration restitution and alternans in rabbit ventricular myocytes: the key role of intracellular calcium cycling. *Circ. Res.* 96:459–466.
16. Zaniboni, M. 2018. Short-term action potential memory and electrical restitution: a cellular computational study on the stability of cardiac repolarization under dynamic pacing. *PLoS One.* 13:e0193416.
17. ten Tusscher, K. H., and A. V. Panfilov. 2006. Alternans and spiral breakup in a human ventricular tissue model. *Am. J. Physiol. Heart. Circ. Physiol.* 291:H1088–H1100.
18. Dvir, H., and S. Zlochiver. 2013. Stochastic cardiac pacing increases ventricular electrical stability–a computational study. *Biophys. J.* 105:533–542.
19. Schaeffer, D. G., J. W. Cain, …, W. Krassowska. 2007. An ionically based mapping model with memory for cardiac restitution. *Bull. Math. Biol.* 69:459–482.
20. Dvir, H., and S. Zlochiver. 2014. The interrelations among stochastic pacing, stability, and memory in the heart. *Biophys. J.* 107:1023–1034.
21. Weiss, J. N., A. Karma, …, Z. Qu. 2006. From pulsus to pulseless: the saga of cardiac alternans. *Circ. Res.* 98:1244–1253.
22. Sato, D., Y. Shiferaw, …, A. Karma. 2006. Spatially discordant alternans in cardiac tissue: role of calcium cycling. *Circ. Res.* 99:520–527.
23. Lemay, M., E. de Lange, and J. P. Kucera. 2012. Uncovering the dynamics of cardiac systems using stochastic pacing and frequency domain analyses. *PLoS Comput. Biol.* 8:e1002399.
24. Prudat, Y., R. V. Madhvani, …, J. P. Kucera. 2016. Stochastic pacing reveals the propensity to cardiac action potential alternans and uncovers its underlying dynamics. *J. Physiol.* 594:2537–2553.
25. Kanaporis, G., and L. A. Blatter. 2015. The mechanisms of calcium cycling and action potential dynamics in cardiac alternans. *Circ. Res.* 116:846–856.
26. Huikuri, H. V., T. Seppänen, …, R. J. Myerburg. 1996. Abnormalities in beat-to-beat dynamics of heart rate before the spontaneous onset of life-threatening ventricular tachyarrhythmias in patients with prior myocardial infarction. *Circulation.* 93:1836–1844.
27. Weinberg, S. H., and L. Tung. 2012. Oscillation in cycle length induces transient discordant and steady-state concordant alternans in the heart. *PLoS One.* 7:e40477.
28. Weinberg, S. H. 2015. Spatial discordance and phase reversals during alternate pacing in discrete-time kinematic and cardiomyocyte ionic models. *Chaos.* 25:103119.
29. O'Hara, T., L. Virág, …, Y. Rudy. 2011. Simulation of the undiseased human cardiac ventricular action potential: model formulation and experimental validation. *PLoS Comput. Biol.* 7:e1002061.
30. Al-Zaiti, S. S., J. A. Fallavollita, …, M. G. Carey. 2014. Electrocardiographic predictors of sudden and non-sudden cardiac death in patients with ischemic cardiomyopathy. *Heart Lung.* 43:527–533.
31. Berenfeld, O. 2018. Computational approaches for accurate rotor localization in the human atria. *In* Cardiac Electrophysiology, From Cell To Bedside., *Volume 35*, Seventh Edition. Elsevier, pp. 335–344.
32. Liao, F., and Y. K. Jan. 2012. Enhanced phase synchronization of blood flow oscillations between heated and adjacent non-heated sacral skin. *Med. Biol. Eng. Comput.* 50:1059–1070.
33. Elstad, M., E. L. O'Callaghan, …, R. Ramchandra. 2018. Cardiorespiratory interactions in humans and animals: rhythms for life. *Am. J. Physiol. Heart Circ. Physiol.* 315:H6–H17.
34. Helfenbein, E., R. Firoozabadi, …, S. Babaeizadeh. 2014. Development of three methods for extracting respiration from the surface ECG: a review. *J. Electrocardiol.* 47:819–825.
35. Kleiger, R. E., J. P. Miller, …, A. J. Moss. 1987. Decreased heart rate variability and its association with increased mortality after acute myocardial infarction. *Am. J. Cardiol.* 59:256–262.
36. Koller, M. L., S. K. Maier, …, R. F. Gilmour, Jr. 2005. Altered dynamics of action potential restitution and alternans in humans with structural heart disease. *Circulation.* 112:1542–1548.
37. Decker, K. F., J. Heijman, …, Y. Rudy. 2009. Properties and ionic mechanisms of action potential adaptation, restitution, and accommodation in canine epicardium. *Am. J. Physiol. Heart Circ. Physiol.* 296:H1017–H1026.
38. Watanabe, M. A., and M. L. Koller. 2002. Mathematical analysis of dynamics of cardiac memory and accommodation: theory and experiment. *Am. J. Physiol. Heart Circ. Physiol.* 282:H1534–H1547.
39. Wu, R., and A. Patwardhan. 2004. Restitution of action potential duration during sequential changes in diastolic intervals shows multimodal behavior. *Circ. Res.* 94:634–641.
40. Berger, R. D. 2004. Electrical restitution hysteresis: good memory or delayed response? *Circ. Res.* 94:567–569.
41. Dvir, H., and S. Zlochiver. 2011. Heart rate variability effect on the myocyte action potential duration restitution: insights from switched systems theory. *Conf. Proc. IEEE Eng. Med. Biol. Soc.* 2011:685–688.